Preparation of glycine mediated graphene oxide/g-C$_3$N$_4$ lamellar membranes for nanofiltration

Zhitao Wu [a], Le Gao [a], Jie Wang [a], Feigang Zhao [a], Longlong Fan [a], Dan Hua [a,**], Susilo Japip [b], Jingran Xiao [a], Xueji Zhang [c], Shu-Feng Zhou [a,***], Guowu Zhan [a,*]

[a] College of Chemical Engineering, Integrated Nanocatalysts Institute (INCI), Huaqiao University, 668 Jimei Avenue, Xiamen, Fujian, 361021, PR China
[b] Department of Chemical & Biomolecular Engineering, National University of Singapore, 4 Engineering Drive 4, 117585, Singapore
[c] School of Biomedical Engineering, Shenzhen University Health Science Center, Shenzhen, Guangdong, 518060, PR China

ARTICLE INFO

ABSTRACT

In this work, we fabricated a series of composite membranes for nanofiltration by filtration-assisted assembly of graphene oxide (GO, with a thickness of *ca.* 2 nm) and graphitic carbon nitride (g-C$_3$N$_4$, with a thickness of *ca.* 5.2 nm) nanosheets with the assistance of glycine as a molecular linker to enhance their interactions. The effects of g-C$_3$N$_4$ and glycine concentrations on the lamellar spacing of GO and membrane performance were subsequently investigated. Interestingly, experimental and characterization results showed that both g-C$_3$N$_4$ and glycine could increase the interlayer spacing of pristine GO membranes, but the former reduced the dimensions of nanochannels while the latter led to enlarged channels. As compared with pristine GO membranes, the composite membranes resulted in faster water transportation without sacrificing solute retention. With further functionalization by introducing hyperbranched polyethyleneimine (HPEI) coating, we demonstrated that an integrated Gly-GO/g-C$_3$N$_4$ membrane (*ca.* 116 nm in thickness) exhibited excellent separation performance for various organic dye solutions under different operational conditions (feed concentration, pH, etc.). Long-term stability experiments showed that this membrane yielded 90%–93% dye rejection with only a slight decline in permeance over a 40 h testing period, indicating acceptable stability. The pure water permeance of the Gly-GO/g-C$_3$N$_4$ membrane reached as high as 207 L h^{-1} m^{-2} bar^{-1}. These results indicate that the covalent modification of small molecules can improve the packing of GO nanosheets and lead to outstanding nanofiltration performance which has great potential applications in the field of water purification and separation.

1. Introduction

Nanofiltration technology has been widely studied for use in drinking water purification and wastewater treatment due to its low energy consumption, easy operation, space-savings, and high efficiency [1]. A myriad of membranes have been developed to maximize both permeability and selectivity during separation processes, but increasing permeability is usually associated with decreasing selectivity, which is known as an inherent trade-off characteristic. In recent years, tremendous research effort has been focused on the self-assembly of graphene and the derivative graphene oxide (GO) materials as membranes to control the trade-off between flux and rejection for satisfying industrial demands [2–5]. Unfortunately, it remains a big challenge to simultaneously access high solvent flux and high solute rejection using a GO membrane.

Two-dimensional (2D) GO has unique hydrophilic property, high specific surface area (up to 2630 m^2/g) [6], excellent mechanical strength, and flexibility due to the presence of a large number of oxygen-containing groups (e.g., carboxyl, hydroxyl, and epoxy groups) on its surface [7,8]. It has been reported that single-layer graphene/GO was impermeable to any liquid/gas molecules in a defect-free state unless interconnected pores/channels with a certain size were created using chemical etching, thermal treatment, or ion bombardment, etc. [9, 10] Recently, Yang et al. prepared a centimeter-scale graphene/carbon nanotube hybrid membrane by oxygen plasma etching to produce relatively uniform nanopores (~0.55 nm), which achieved a high salt

* Corresponding author.
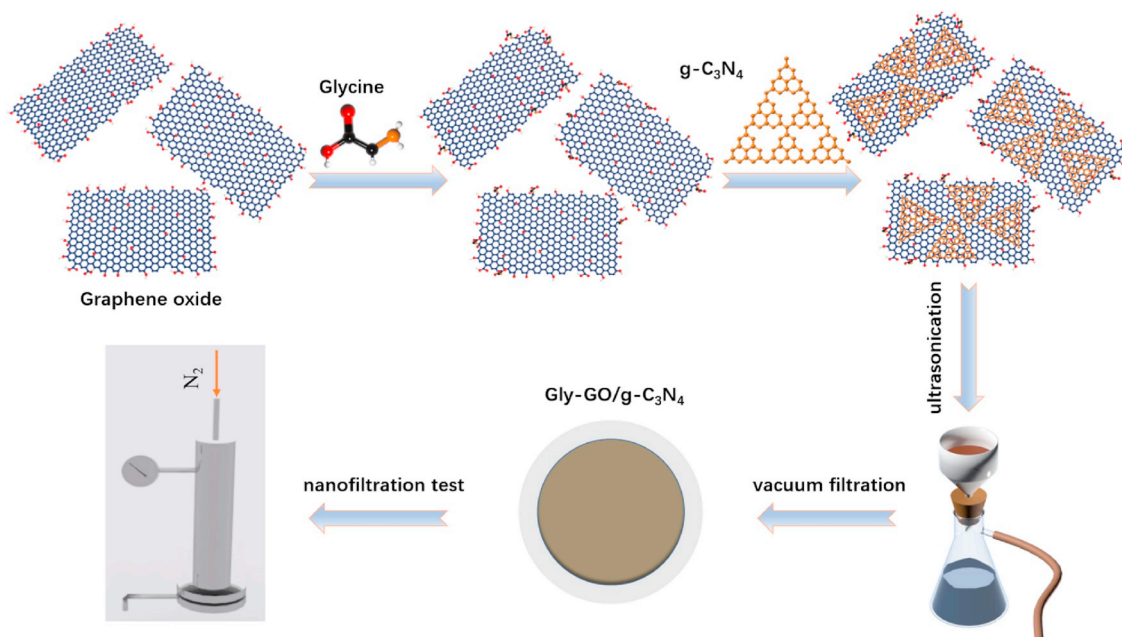** Corresponding author.
*** Corresponding author.
E-mail addresses: huadan@hqu.edu.cn (D. Hua), szhou@hqu.edu.cn (S.-F. Zhou), gwzhan@hqu.edu.cn (G. Zhan).

Scheme 1. The preparation process of Gly-GO/g-C$_3$N$_4$ composite membranes for nanofiltration.

rejection rate up to 97% [11]. However, the current strategies for engineering pores in GO do not allow fine-control of pore size and in general, result in the reduction of mechanical strength or the formation of defects in a single-layer GO membrane.

In a multilayer GO membrane, adjacent nanosheets can form 2D empty space that allows water (smaller than the size of the channels) to pass into the non-oxidized regions, while the oxidized regions serve as spacers for the 2D capillary networks [12]. A closely packed GO membrane can be prepared by vacuum filtration, drop-casting, and spray- or spin-coating, etc. [13] For instance, Han et al. prepared an ultrathin GO membrane by vacuum filtration. The formed 2D nanopores maintained a high permeance of 21.8 L h^{-1} m^{-2} bar^{-1} for pure water and exhibited a 99% rejection of organic dyes [14]. Goh et al. adopted the dip-coating technique to immobilize GO on a PEI-modified hollow fiber membrane, which not only improved the mechanical properties but also improved the permeability for pure water [15]. However, the relatively low permeability and stability of the multilayer GO membranes still limit their practical applications.

It is well-known that the interlaminar structure of GO provides a perfect scaffold for embedding guest materials [16], thus many polymers or nanomaterials have been encapsulated in the interlayer space to modify GO membranes [17]. For instance, Chen et al. reported inserting TiO$_2$ nanoparticles between GO layers to increase water flux while maintaining organic dye rejection [18]. Ran et al. developed a method for intercalating ionic polymers into the space between neighboring GO nanosheets via non-covalent interactions, and the resultant membrane showed improved water flux (2.5 L m^{-2} h^{-1}) and longer stability [19]. Furthermore, small molecules are frequently used in the modification of GO membranes via covalent bonds. For instance, Huang et al. adopted a diamine monomer to crosslink adjacent GO sheets. Although the stability of the obtained GO membrane was enhanced, the demonstrated water flux was not robust [20].

Graphitic carbon nitride (g-C$_3$N$_4$) is another type of 2D material with a π-conjugated graphite planar structure formed by carbon and nitrogen sp^2 hybridization [17]. Recently, a variety of hybrid membranes with g-C$_3$N$_4$ and GO have been fabricated due to their good compatibility [21–23]. In this study, we report a new method for assembling 2D GO/g-C$_3$N$_4$ nanosheets via a glycine modification method. As shown in Scheme 1, the preparation of a glycine-mediated GO/g-C$_3$N$_4$ composite membrane (Gly-GO/g-C$_3$N$_4$) was mainly divided into three steps: (i)

graphene oxide was functionalized with glycine by amide bonds under the action of a catalyst, (ii) integration of g-C$_3$N$_4$ and Gly-GO by sonication followed by assembly via filtration, and (iii) further surface modification by hyperbranched polyethyleneimine (HPEI) to adjust the membrane surface charge. Several dye/water mixtures were then used as model solutions to evaluate the separation performance of the obtained membranes. At the same time, the effects of the amount of glycine and g-C$_3$N$_4$ and the molecular weight of HPEI on the membrane properties were also investigated. A series of characterizations were adopted to elucidate the relationships between the structural properties and separation performance of the composite membranes.

2. Experiment methods

2.1. Materials

A GO aqueous solution at a concentration of 5000 ppm was purchased from Angstron Materials (US). Mixed cellulose ester microporous substrates (MCE, 47 mm in diameter and 0.22 μm in pore diameter) were purchased from Beijing Xinweier Glass Instrument. Anodic aluminum oxide membrane (AAO, 47 mm in diameter and 0.22 μm in pore size) was purchased from Whatman (US). Hyperbranched polyethyleneimine (HPEI) was purchased from Adamas, at three different molecular weights (M.W.) of 600, 1800, and 10,000, respectively. Glycine and melamine were purchased from Sinopharm (China). The 1-(3-dimethylaminopropyl)-3-ethylcarbodiimide hydrochloride (EDC) and N-hydroxysuccinimide (NHS) were both purchased from Aladdin. In addition, five different dyes, namely, methylene blue (MB), rhodamine B (RhB), Eosin Y (EY), Evans blue (EB), and Alcian blue 8GX (AB), were purchased from commercial suppliers and used as received without pretreatments. Deionized water was used in all of the experiments.

2.2. Preparation of g-C$_3$N$_4$ nanosheets

g-C$_3$N$_4$ was synthesized using melamine as a raw material based on a previous report [24]. Specifically, 2.5 g of melamine was calcined in air at 550 °C for 3 h with a ramping rate of 3 °C/min, then the obtained yellow powder was ground in a mortar, before soaking at 500 °C for 2 h in an N$_2$ atmosphere with a heating rate of 3 °C/min. Subsequently, 50 mg of the obtained powder was re-dispersed in 30 mL of HCl (12 M), and
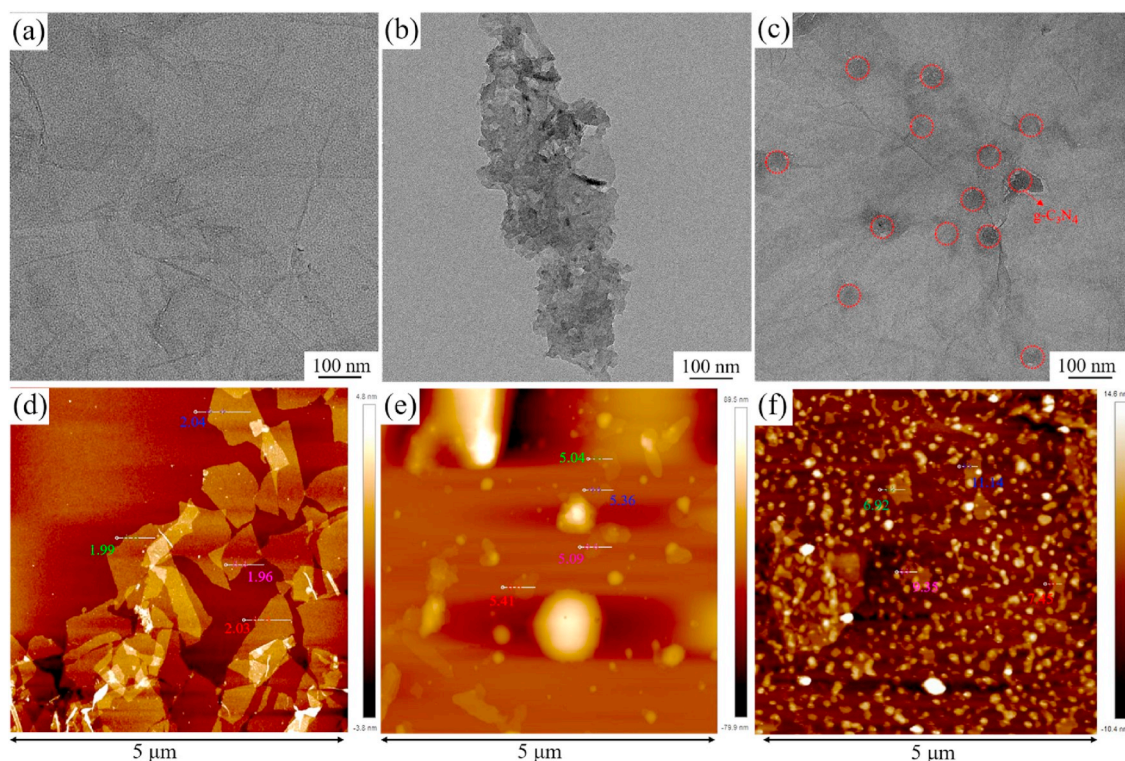
Fig. 1. TEM images of (a) GO nanosheets, (b) g-C$_3$N$_4$ nanosheets, and (c) GO/g-C$_3$N$_4$ composite. AFM images of (d) GO nanosheets, (e) g-C$_3$N$_4$ nanosheets, and (f) GO/g-C$_3$N$_4$ composite.

the mixture was heated at 50 °C for 12 h. Afterwards, the mixture was filtered through a filter (pore size of 0.45 μm) and washed with deionized water several times to remove excess HCl. The white-colored product was then re-dispersed in 200 mL of deionized water by sonication for 2.5 h in an ice bath. Finally, the solution was centrifuged three times at 5000 ppm for 10 min each time to remove bulk particles. The concentration of g-C$_3$N$_4$ in the obtained supernatant was 150 ppm as determined using an UV–vis spectrophotometer (Metash, UV-8000).

2.3. Preparation of GO/g-C$_3$N$_4$ composite membranes

The composite membranes were fabricated by vacuum filtration onto MCE substrates. In brief, the original GO dispersion was diluted with deionized water to a final concentration of 100 ppm. Then, 2 mL of the GO dispersion (100 ppm) was mixed with different volumes of g-C$_3$N$_4$ (1.0, 1.5, or 2.0 mL). The volume of the mixture was maintained at 20 mL by adding water before sonication treatment for 1 h. Afterwards, the GO/g-C$_3$N$_4$ dispersion was vacuum filtered onto MCE substrates.

2.4. Preparation of glycine modified GO/g-C$_3$N$_4$ composite membrane

Similarly, 2 mL of the GO dispersion (100 ppm) was added to 14 mL of deionized water. Then 300 μL of EDC (1 mg/L) and NHS (0.5 mg/L) were successively added to the GO dispersion to activate the carboxyl groups on the GO surface. After 15 min, a glycine solution (1 mg/mL) was added and the solution was stirred for 12 h. After the reaction was completed, 2 mL of the above-prepared g-C$_3$N$_4$ aqueous solution was added to the mixture under sonication for 1 h, and the mixture was then vacuum filtered to form a membrane. For the HPEI modified membranes, the freshly prepared membranes were immersed in a 1 wt% aqueous solution of HPEI for 0.5 h, and then the membrane was rinsed with deionized water by soaking in a beaker for 10 s.

2.5. Separation performance evaluation

A home-made filtration set-up was used to evaluate the membrane performance (refer to Fig. S1). The membrane permeation (P) can be expressed as follows:

$$P = \frac{V}{t \times A \times \Delta p}$$

In the formula, V represents the volume of the filtrate (L), t represents the filtration time (h), A represents the effective filtration area of the membrane (herein, 3.462 cm^2), and Δp represents the pressure difference as the driving force (bar). The solute rejection rate (R) was calculated as follows:

$$R = \left(1 - \frac{C_P}{C_F}\right) \times 100\%$$

C_F and C_P represent the solute concentrations in the feed and permeate, respectively, which were measured by an UV–vis spectrophotometer (Metash, UV-8000) at a certain wavelength. For instance, the characteristic absorption peaks of MB, RhB, EY, EB, and AB are 664.5 nm, 554 nm, 516 nm, 623 nm, and 614 nm, respectively.

2.6. Characterization techniques

The surface and cross-section of the samples were observed by scanning electron microscope (SEM, ZESSIS, EVO®18) and transmission electron microscope (TEM, FEI, Talos F200S). The surface roughness of the composite membrane was determined by atomic force microscopy (AFM, Bruker, MultiMode 8). The chemical composition and bonding information of the membrane were obtained using a Fourier transform infrared spectroscopy (FTIR, Thermo, Nicolet iS50) and an X-ray photoelectron spectroscopy (XPS, Thermo, ESCALAB 250XI). The surface charge of the dispersion solution was measured with ZETA potential analyzer (Bruker, NanoBrook Omni). N$_2$ adsorption-desorption
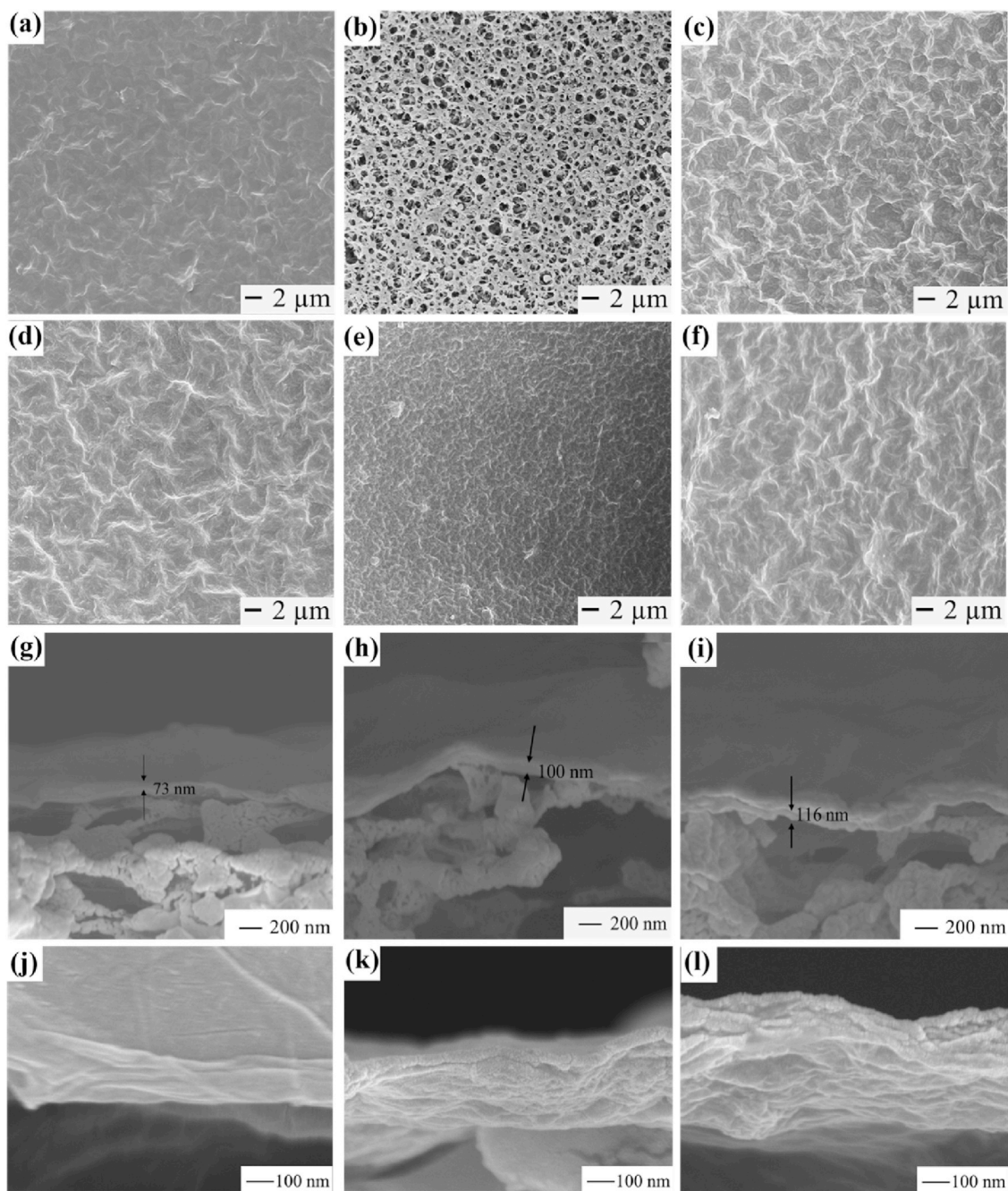
Fig. 2. Representative SEM images of different membranes. The top view images of (a) GO membrane, (b) g-C$_3$N$_4$ membrane, (c) GO/g-C$_3$N$_4$ membrane, (d) GO/g-C$_3$N$_4$ membrane modified by HPEI, (e) Gly-GO/g-C$_3$N$_4$ membrane, and (f) Gly-GO/g-C$_3$N$_4$ membrane modified by HPEI. The cross-section view images of (g, j) GO membrane, (h, k) GO/g-C$_3$N$_4$ membrane, and (i, l) Gly-GO/g-C$_3$N$_4$ membrane.

isotherms of the membrane samples were acquired using a physisorption instrument (Quantachrome, Autosorb-iQ) at 77 K, wherein the membrane samples were freeze-dried and peeled off from the MCE substrate before the measurement. In addition, the membrane microstructure was studied by a positron annihilation spectroscopy (PAS) called Doppler broadening energy spectroscopy via a slow beam positron apparatus. S parameter curves as a function of positron incident energy obtained from PAS can be used to analyze the microstructural changes along with the membrane depth profile. The S parameter reflects the free volume properties, while the incident positron energy is related to the mean depth of the materials by the following equation:

$$Z(E_+) = \left(\frac{40}{\rho}\right) \times E_+^{1.6}$$

Wherein Z is the mean depth (nm), ρ is the material density (g cm^{-3}), and E_+ is the incident positron energy (keV).

3. Results and discussion

3.1. Characterizations of GO/g-C$_3$N$_4$ composite membranes

As shown in the TEM images in Fig. 1, both g-C$_3$N$_4$ and GO were produced in a nanosheet shape. The GO nanosheets have clear edges and wrinkles, indicating a thin film morphology. For comparison, the lateral
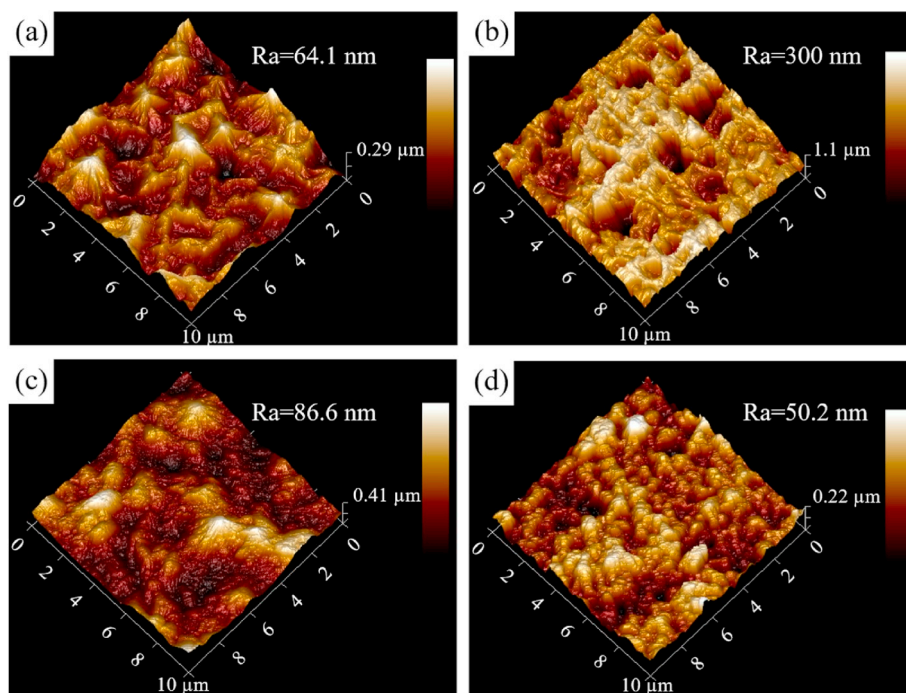
Fig. 3. Representative AFM images of different membranes. (a) GO membrane, (b) g-C$_3$N$_4$ membrane, (c) GO/g-C$_3$N$_4$ composite membrane, and (d) Gly-GO/g-C$_3$N$_4$ composite membrane.

size of the GO nanosheet was much larger than that of the g-C$_3$N$_4$ nanosheet, due to the fact that GO contains more oxygen-containing groups (*e.g.,* –OH, –COOH, etc.), facilitating its dispersion in water [25]. In the resulting GO/g-C$_3$N$_4$ composite, the exfoliated g-C$_3$N$_4$ nanosheet was uniformly distributed over the GO nanosheets. Fig. 1d–f presents AFM images of GO, g-C$_3$N$_4$, and their hybrid samples, respectively. As shown here, the GO and g-C$_3$N$_4$ nanosheets have an average thickness of 2 nm and 5.2 nm, respectively. As the theoretical thicknesses of monolayer GO and monolayer g-C$_3$N$_4$ are 0.7 nm and 0.326

nm, respectively [26,27], this suggests that most GO nanosheets used in this work have three layers, while the majority of heptazine-based g-C$_3$N$_4$ nanosheets are 16-layered. Regarding the composite sample, the thickness was in the range of 7–11 nm due to the stacking of two different nanosheets.

Subsequently, the nanosheet-like GO and g-C$_3$N$_4$ were assembled through vacuum filtration of an aqueous dispersion on an MCE substrate. A pure GO membrane displayed a pronounced wrinkle morphology [28], and no obvious defects can be found as shown in
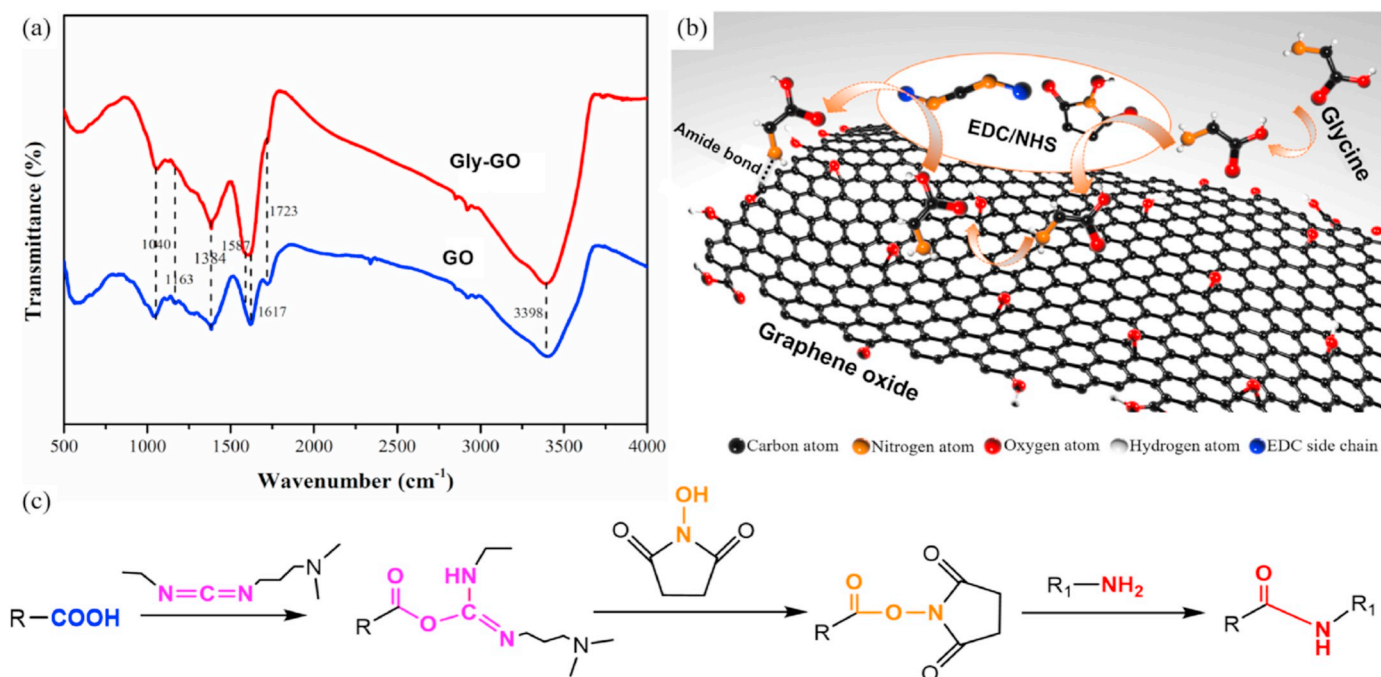
Fig. 4. (a) FTIR spectra of the pristine GO sample and glycine modified GO sample. (b) The schematic illustration of the formation of amide bonds from glycine and GO, and (c) the activation process of carboxyl groups using EDC/NHS as a catalyst.
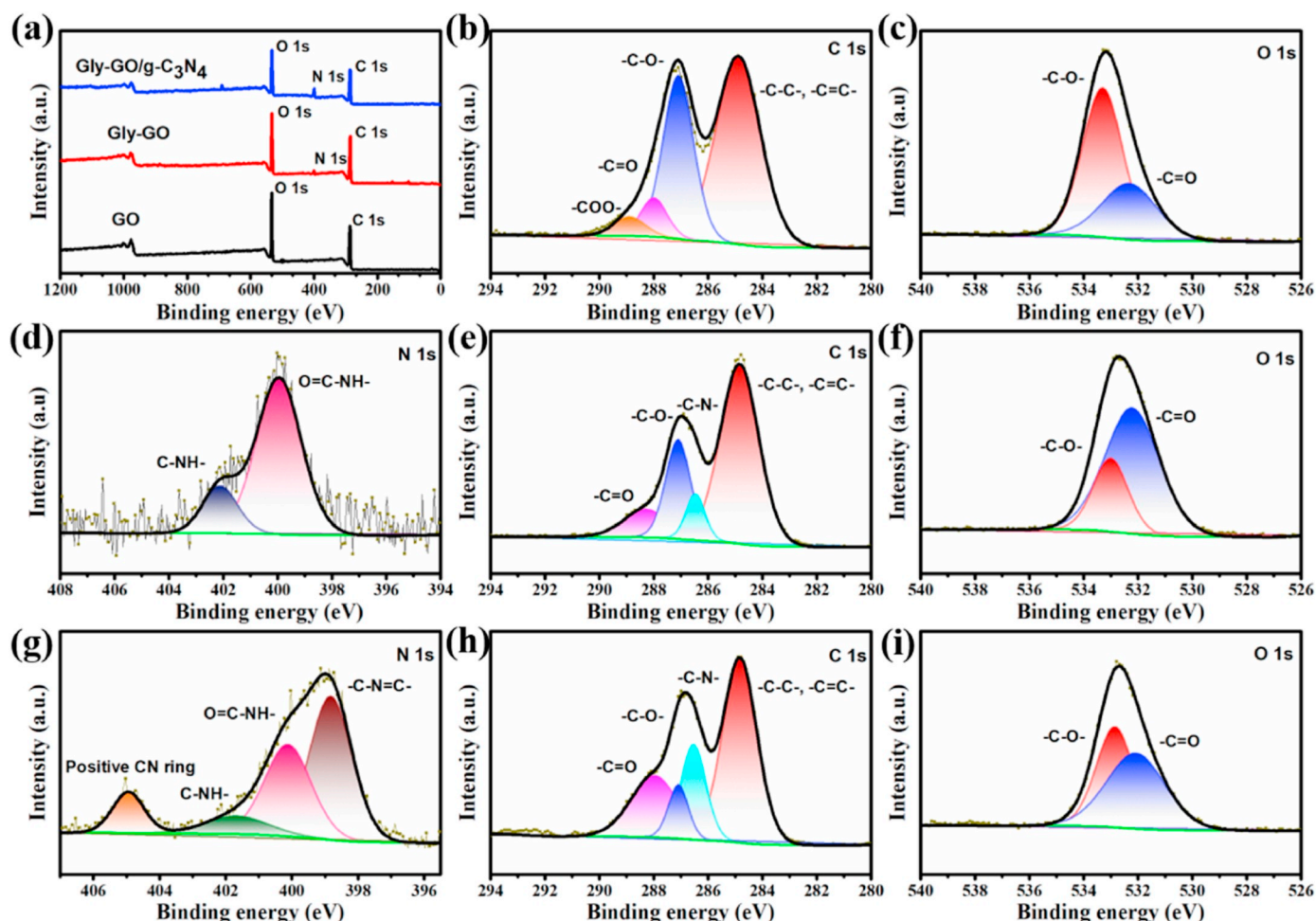
Fig. 5. XPS spectra of (a) survey, (b) C 1s, and (c) O 1s of GO membrane, (d) N 1s, (e) C 1s, and (f) O 1s of Gly-GO membrane, (g) N 1s, (h) C 1s, and (i) O 1s of Gly-GO/g-C$_3$N$_4$ membrane.

Fig. 2a. For comparison, the surface of a pure g-C$_3$N$_4$ membrane (Fig. 2b) only exhibited the porous structure of the MCE substrate (also see Fig. S2), suggesting that g-C$_3$N$_4$ nanosheets alone could not form an intact membrane. As shown in Fig. S3, the zeta potentials of GO and g-C$_3$N$_4$ suspensions were −19.85 and 22.86 mV, indicating that their dispersions were negatively and positively charged, respectively. Thus, the interactions between GO and g-C$_3$N$_4$ in the composite membranes are mainly due to electrostatic force and π-π stacking interaction [17, 23]. In addition, GO/g-C$_3$N$_4$ and Gly-GO/g-C$_3$N$_4$ membranes (see Fig. 2c and e) retained the typical wrinkle structure of GO. The XRD patterns of the membranes are shown in Fig. S4, and two pronounced diffraction peaks at 13.1° and 27.4° were present for g-C$_3$N$_4$, while a characteristic peak at 10.8° was present for GO. However, the XRD patterns of GO-based membranes show no diffraction peaks related to stacked GO nanosheets, implying the formation of a loosely stacked microstructure. This phenomenon was similar to a report showing that a solvated GO membrane did not exhibit the characteristic peaks at 2θ < 16° [29]. In contrast, if membranes showed XRD peaks associated with stacked GO sheets with 2θ between 5° and 13°, they showed low permeance due to a compact microstructure as suggested in this report.

As can be clearly seen from Fig. 2g, h, i, the cross-sectional SEM images indicate the varying thickness of the GO/g-C$_3$N$_4$ and Gly-GO/g-C$_3$N$_4$ membranes, which are 100 nm and 116 nm, respectively, and both are greater than that of pure GO membrane (73 nm). The reason was that the insertion of g-C$_3$N$_4$ and glycine changed the layer spacing of the GO nanosheets. In addition, we found that HPEI coating did not bring about any significant change in the surface of the composite membrane, as

shown in Fig. 2d, f. Moreover, Fig. 2j-l clearly shows the lamellar features of membranes created by the self-assembled nanosheet materials. Both the intercalation of g-C$_3$N$_4$ and glycine significantly increased the thickness of the selective layer.

The surface morphology of the membranes was also studied by AFM, as displayed in Fig. 3. As shown, all of the membranes exhibited a typical hills and valleys morphology. Statistical analysis shows that the average roughness (Ra) of pure GO membrane was 64.1 nm. The nodular surface morphology was also found for pure g-C$_3$N$_4$ membrane, but it had a much higher Ra of 300 nm. Interestingly, the Ra value of the hybrid GO/g-C$_3$N$_4$ membrane became 86.6 nm. These results indicate that the insertion of g-C$_3$N$_4$ affected the laminar structure of the GO membrane, which increased the roughness of the membrane surface. However, when glycine was introduced in the hybrid membrane, the average roughness decreased to 50.2 nm, which suggested that the chemical modification of GO nanosheets by glycine facilitated the assembly of GO and g-C$_3$N$_4$ [30].

The surface organic groups of pristine GO and glycine-modified GO were next compared by FTIR. As can be seen from Fig. 4a, the four characteristic absorption bands of pristine GO correspond to the stretching vibration of epoxy group (1040 cm^{-1}), the bending vibration of hydroxyl group (1384 cm^{-1}), the stretching vibration of benzene ring (1617 cm^{-1}), and the stretching vibration (1723 cm^{-1}) of carboxyl group [7,25,31]. In the Gly-GO sample, the N–H characteristic band overlaps with the stretching vibration band of O–H at 3398 cm^{-1} [32, 33], and a new band appears around 1587 cm^{-1}, which can be attributed to the bending vibration of N–H group [34,35]. In addition, the
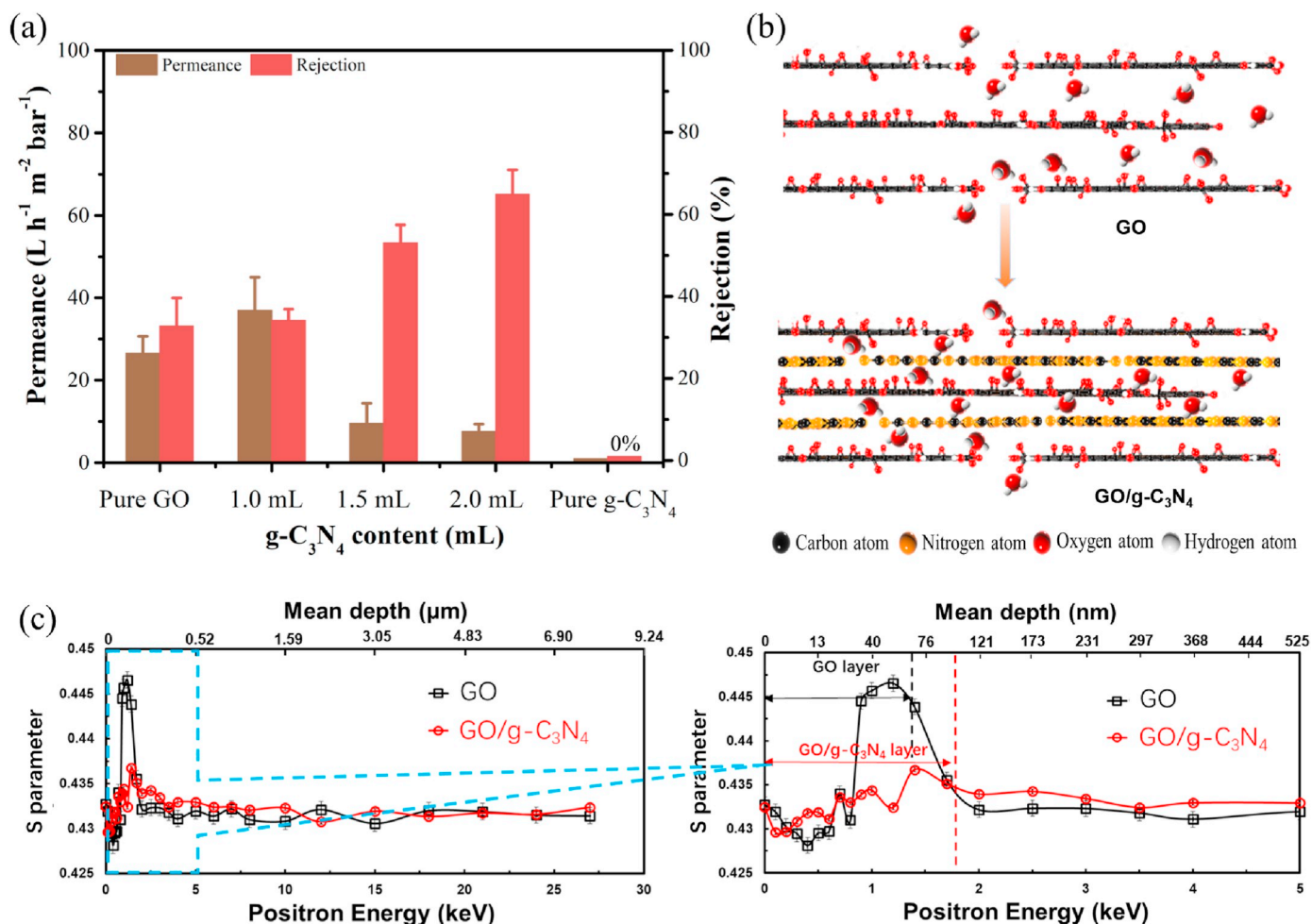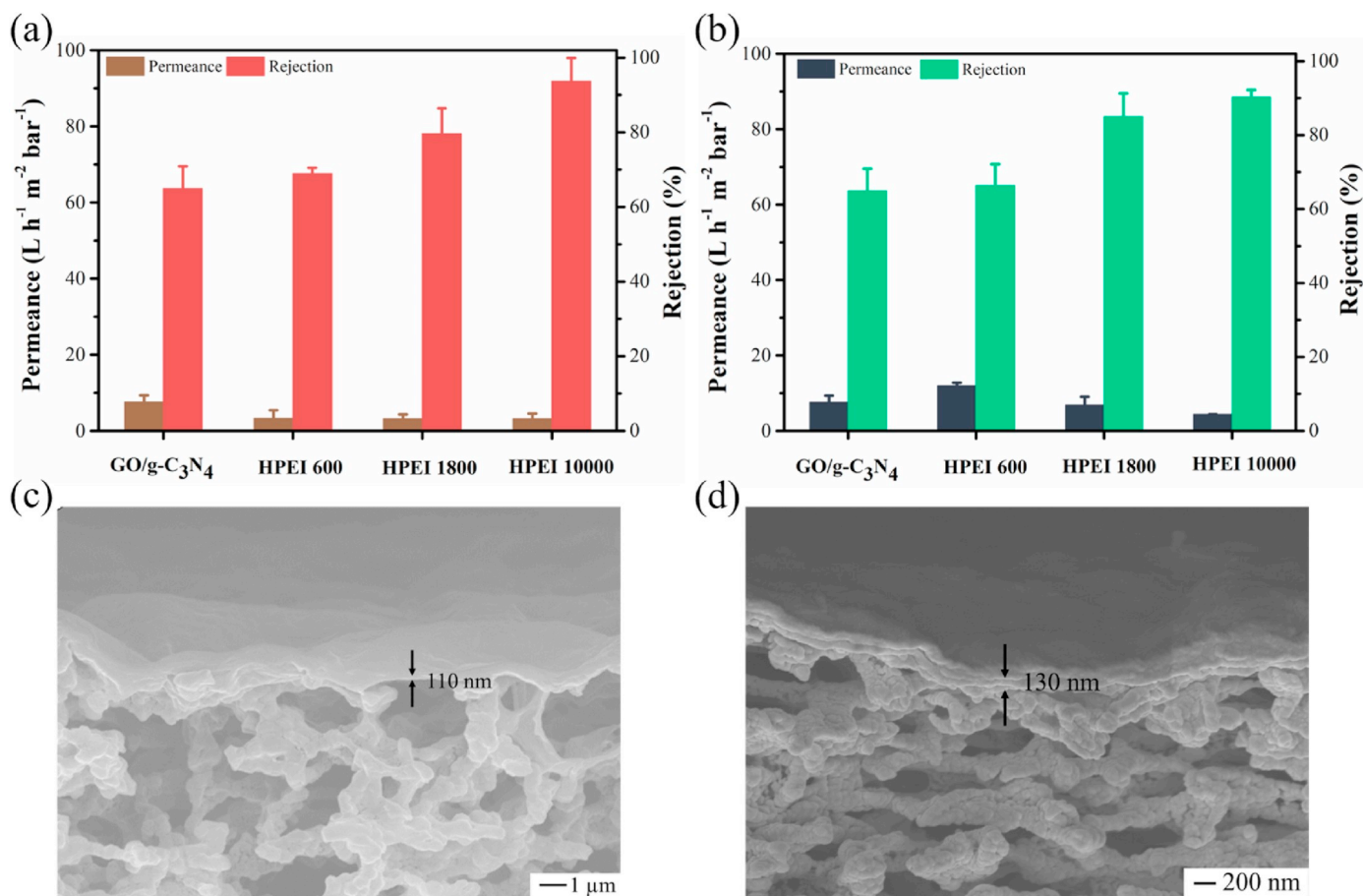
Fig. 6. (a) Separation performance of GO/g-C$_3$N$_4$ composite membranes with different loading of g-C$_3$N$_4$. (b) Schematic diagram of water molecules passing through 2D nanochannels before and after g-C$_3$N$_4$ was inserted into the GO layers. (c) S parameter curves of the pristine GO and GO/g-C$_3$N$_4$ membranes.

relative intensities of the FTIR absorption bands were also changed, especially the absorption intensity of the carboxyl group, which was significantly reduced after glycine modification. This was caused by the formation of amide bonds due to catalyzation with EDC and NHS (see Fig. 4b and c) [20]. Specifically, in an aqueous solution, EDC can react with carboxyl groups on the GO surface to form an active intermediate, which then reacts with an amino group on glycine to form an amide bond. However, the active intermediate is unstable; therefore, NHS was added to prevent the intermediate from being hydrolyzed, effectively increasing the reaction yield. Since the amount of glycine was not sufficient to completely react with all of the carboxyl groups on GO, the absorption band of the amide group was not remarkable in the FTIR spectra. As a result, there was only a weak absorption band at 1651 cm^{-1}, which corresponded to the carbonyl group in the amide group [36].

In order to gain insight into the bonding environment and surface chemical composition of the membranes, XPS surveys and narrow scans were conducted. Fig. 5a displays the XPS survey spectra of GO, Gly-GO and Gly-GO/g-C$_3$N$_4$ samples. Clearly, the pure GO did not contain nitrogen, and the nitrogen signal was found only in Gly-GO and Gly-GO/g-C$_3$N$_4$ samples. The nitrogen content in the Gly-GO and Gly-GO/g-C$_3$N$_4$ samples was 2.6 at% and 9.7 at%, respectively (see Table S1). The C 1*s* peak in the GO sample could be deconvoluted into different components with binding energies (BEs) of 284.8, 287, 287.9 and 288.9 eV that could be assigned to –C═C–/–C-C-, -C-O-, –C═O, and -COO-, respectively [9, 37,38]. These results confirmed that there were abundant carboxylic groups on the GO surface. Likewise, in the Gly-GO sample, the C 1*s*

spectrum could be deconvoluted into peaks at 284.8, 286.6, 287, and 288.5 eV, which could be assigned to –C═C–/–C-C-, -C-N-, -C-O-, and –C═O, respectively. The presence of -C-N- implied the successful surface functionalization of glycine molecules on the GO surface [22]. As expected, the ratio of -C-N- in total C in Gly-GO/g-C$_3$N$_4$ was increased to 18.7%, which was much higher than the 7.6% found in the Gly-GO membrane. The O 1s spectra could be fit into two peaks located at BEs of 532.5 and 533.5 eV, corresponding to –C═O- and -C-O-, respectively, and these were identical between the three samples (see Fig. 5c, f, i). However, the amount of –C═O- was highest in the Gly-GO sample, which was probably caused by the residual glycine molecules on the GO surface. The high-resolution N 1*s* spectra of the Gly-GO and Gly-GO/g-C$_3$N$_4$ samples are shown in Fig. 5d, g, respectively. The N 1*s* peaks in Gly-GO could be assigned to O═C–NH- (399.9 eV) and -C-NH- (amino group, 402.1 eV) [23]. In contrast, the N 1*s* peaks in Gly-GO/g-C$_3$N$_4$ had more species, including -C-N═C (398.7 eV), O═C–NH- (400 eV), -C-NH- (402 eV), and a positive C–N ring (404.9 eV), respectively [35,39,40]. The presence of both –C═N and the positive C–N ring were caused by the addition of g-C$_3$N$_4$ (*i.e.*, the triazine ring structure). In addition, the XPS was also used to analyze the interaction between g-C$_3$N$_4$ and glycine. The C 1*s* spectra of pure g-C$_3$N$_4$ and Gly-g-C$_3$N$_4$ samples (Figs. S5a and c), showed three distinguishable peaks at binding energies of 284.8, 286.5, and 288.2 eV, respectively, corresponding to adventitious hydrocarbon, C–O species, and the sp^2-bonded C (*viz.*, N–C═N) of the triazine units in g-C$_3$N$_4$ [41]. It can be seen that a slightly increased amount of C–O was caused by the modification of glycine on g-C$_3$N$_4$. Similarly, in the case of the N 1*s* spectra (Figs. S5b and d), the intensity

Fig. 7. (a,b) Separation performance of GO/g-C$_3$N$_4$ composite membranes modified by HPEI of different molecular weights. (c,d) Representative SEM cross-section image of composite membrane modified by HPEI (M.W. = 10,000). (a,c) Membranes in dry state, and (b,d) membranes in the wet state. Note: herein, 2.0 mL of g-C$_3$N$_4$ was added during the synthesis.

of the peak at 400.0 eV corresponding to the ternary N-(C)$_3$ group increased while the intensity of the peak at 401.2 eV corresponding to the terminal N (*viz.*, C–N–H) decreased. Both pieces of evidence confirm the existence of chemical interactions between the carboxylic groups in glycine and the amino groups in g-C$_3$N$_4$.

3.2. Nanofiltration performance of GO/g-C$_3$N$_4$ composite membranes

3.2.1. The effect of the loading of g-C$_3$N$_4$

As GO and g-C$_3$N$_4$ can be assembled to form an intact membrane by π-π interaction and electrostatic interaction [42,43], the nanofiltration performance was evaluated using an MB/water (20 ppm) solution as a model feed. First, the separation performance of a series of composite membranes prepared by different loading of g-C$_3$N$_4$ was studied, and the results are summarized in Fig. 6a. As shown there, the MB rejection of pure GO membrane was only 32.8% with a total permeance of 26.6 L m^{-2} h^{-1} bar^{-1}. The pure g-C$_3$N$_4$ membrane with its loosely stacked structure exhibited negligible separation performance. However, after the introduction of g-C$_3$N$_4$, the rejection rate was significantly improved. We found that the performance was inversely proportional to the loading of g-C$_3$N$_4$. For example, the MB rejection reached 64.9% by adding 2 mL of g-C$_3$N$_4$ during membrane preparation (*i.e.*, the mass ratio of g-C$_3$N$_4$/GO was *ca.* 1.5), but a reduced permeance of only 7.6 L h^{-1} m^{-2} bar^{-1} was obtained. The reason may be due to the reduced nanochannel dimensions as g-C$_3$N$_4$ nanosheets were intercalated between the layers of GO (see Fig. 6b), leading to slower diffusion of water through the layer. When a higher amount of g-C$_3$N$_4$ was distributed between the laminates, the 2D nanochannels were further reduced in size, resulting

in a higher retention of the MB. In addition, the positively charged g-C$_3$N$_4$ provided a repulsive force to the positive charge dye MB molecules, which also contributed to the better rejection of MB [44,45]. Yet, the effect of adsorption on the separation data was eliminated during the stabilization period. Fig. 6c shows the S parameter and the corresponding penetration depth of positrons over pure GO and GO/g-C$_3$N$_4$ membranes as a function of positron incident energy. As shown here, the GO/g-C$_3$N$_4$ membrane had smaller S values than the pure GO membrane near the peak at 1.2 keV, indicating either a smaller free volume size or a lower free volume content [46,47]. Accordingly, the GO/g-C$_3$N$_4$ membrane possessed a denser structure than the pure GO membrane, which favored a higher rejection of MB. However, the S parameter of the GO/g-C$_3$N$_4$ membrane decreased slower than the pure GO membrane at positron energies >1.2 keV, indicating that it had a thicker selective layer, which was consistent with the above observations from SEM (see Fig. 2 g, h). Therefore, both a denser and thicker selective layer led to the lower permeance and high MB rejection of the GO/g-C$_3$N$_4$ membrane.

3.2.2. The effect of HPEI coating

HPEI is a polymer containing a large number of amino groups, which is frequently used to change the surface charge of a membrane [45], thereby changing the permeability of the membrane. We therefore tested if the separation performance of GO/g-C$_3$N$_4$ composite membranes could be further improved by coating with HPEI of different molecular weights (M.W.), as displayed in Fig. 7. Fig. 7a and b shows the separation performance of the modified membranes in their dry state and wet states (*viz.*, solvated state). From Fig. 7a and b, the laminates were vacuum-tight in the dry state before testing (*i.e.*, without solvent
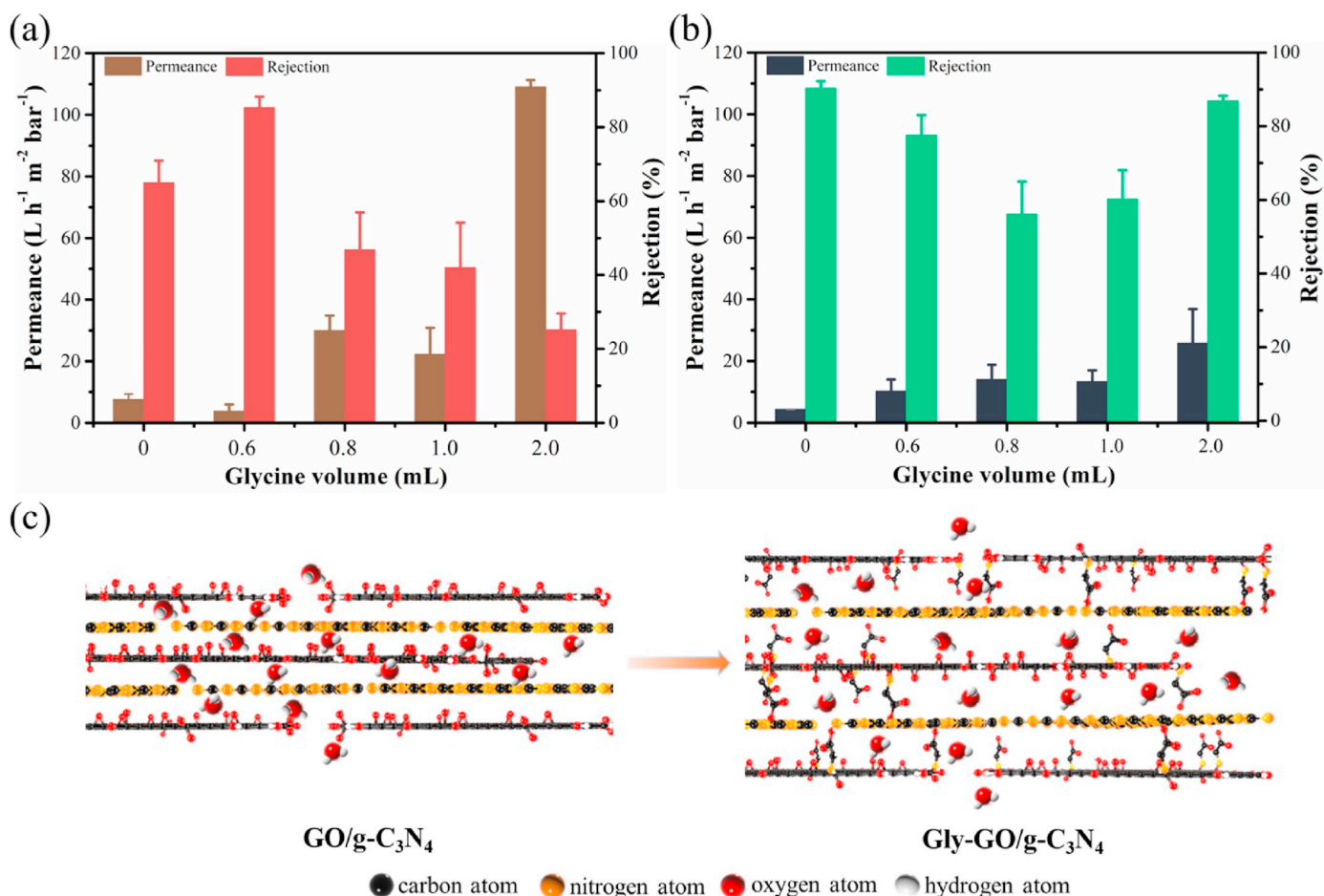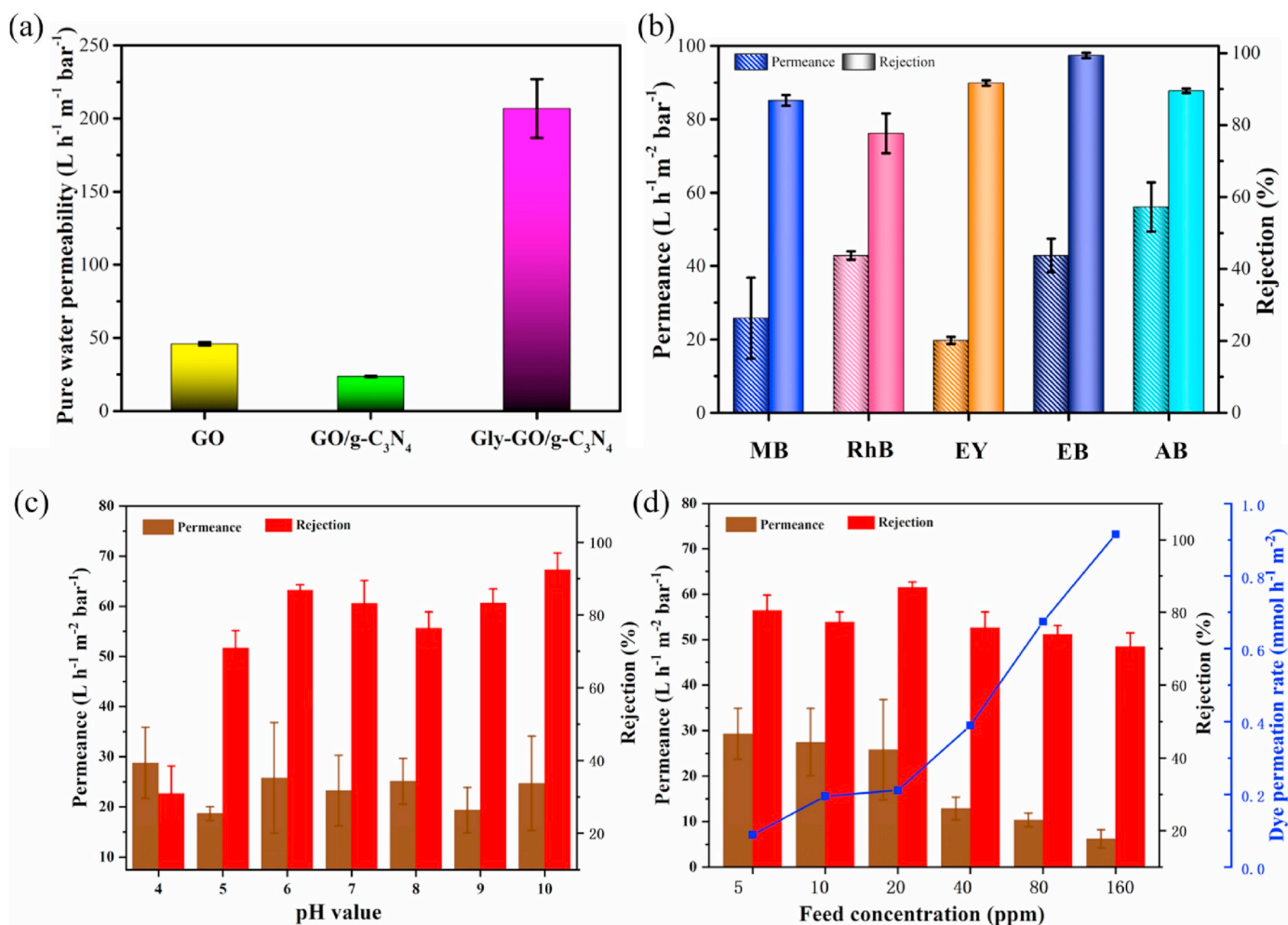
Fig. 8. (a) The separation performance of Gly-GO/g-C$_3$N$_4$ membranes, (b) the separation performance of HPEI modified Gly-GO/g-C$_3$N$_4$ membranes (M.W. of HPEI = 10,000), wherein, the concentration of glycine used in these experiments was 1 mg/mL. (c) Schematic diagram of the process of water passing through 2D nanochannels before and after glycine was inserted into the composite membranes.

soaking), and they showed much lower permeance than the laminates that were soaked in water before testing. For instance, the total permeance of GO/g-C$_3$N$_4$ membrane coated by HPEI (M.W. = 600) was 3.2 and 12.0 L h^{-1} m^{-2} bar^{-1}, respectively, in the dry and wet states. This may be due to the compact microstructure and narrow 2D microchannels in the dried laminates. There was no significant difference in the top-view SEM images of the membranes in the dry state and in the wet state (Fig. S6). However, as shown in the side-view images in Fig. 7c and d, the thickness of the wet membrane (note: freeze-dried before the measurement) is greater than the dry membrane thickness (130 nm vs. 110 nm). By changing the M.W. of HPEI, a similar trend was found (Fig. S7). This finding was consistent with Shi et al. who reported that solvated r-GO membranes showed much higher solvent permeances than completely dried rGO membranes [29]. In addition, the MB rejection increased with increasing M.W. of HPEI in both wet and dried membranes. For instance, the MB rejection was nearly 90% after being coated with HPEI with a M.W. of 10,000. This was due to the positively charged surface deposited by the HPEI coating layer, which produced an additional repulsive force acting on MB molecules as they passed through the 2D channels.

3.2.3. The effect of the amount of glycine

In order to determine the optimal amount of glycine during chemical modification, we also prepared several different membranes with different amounts of glycine, as shown in Fig. 8a. When an increased amount of glycine was used, the permeation and MB rejection were significantly changed. That is, the permeation increased continuously

and the MB rejection decreased. For instance, when 0.6 mL glycine was used, the membrane exhibited an MB rejection of 85.3% and a permeation of 3.8 L h^{-1} m^{-2} bar^{-1}. However, when the amount of glycine was 2 mL, the permeation reached 109.1 L h^{-1} m^{-2} bar^{-1}, which was much larger than the penetration of the GO/g-C$_3$N$_4$ composite membrane. Unfortunately, a very low MB rejection of 25.8% was achieved. Similarly, Fig. S8 shows the S parameter and the corresponding penetration depth of positrons over GO/g-C$_3$N$_4$ and Gly-GO/g-C$_3$N$_4$ membranes as a function of positron incident energy. As shown in Fig. S8, the Gly-GO/g-C$_3$N$_4$ membrane shows a larger S value than the GO/g-C$_3$N$_4$ membrane before 4 keV, indicating its higher free volume or larger pore size. Moreover, the S parameters of the two membranes decreased similarly, indicating the thicknesses of their selective layers were very close. In addition, the pore volume and pore size distribution data of the membrane samples were determined by nitrogen physisorption testing. The results are shown in Fig. S9. Before testing, the GO-based membranes were peeled off from the MCE substrate to obtain information on the selective layer. As shown, all of the GO-based membranes had abundant micropores (pore size < 2 nm), and the average pore sizes of the GO, GO/g-C$_3$N$_4$, and Gly-GO/g-C$_3$N$_4$ membranes were 2.6, 2.2, and 2.8 nm, respectively. The total pore volumes of the GO, GO/g-C$_3$N$_4$, and Gly-GO/g-C$_3$N$_4$ membranes were 0.44, 0.48, and 1.15 cm^3 g^{-1}, respectively. In addition, the specific Brunauer–Emmett–Teller (BET) surface areas of the GO, GO/g-C$_3$N$_4$, and Gly-GO/g-C$_3$N$_4$ membranes were 224, 271, and 589 m^2 g^{-1}. Accordingly, all of the textural properties indicated that the addition of glycine as a molecular linker to GO/g-C$_3$N$_4$ composite membrane increased the pore size and pore volume, thereby enhancing

Fig. 9. (a) Pure water permeance of different membrane at a pressure of 1 bar. (b) Separation performance of Gly-GO/g-C$_3$N$_4$ membranes modified by HPEI (M.W. = 10,000) towards different organic dyes. Note: the amounts of both g-C$_3$N$_4$ and glycine during the synthesis were 2.0 mL. (c) The effect of pH of MB solution on the separation performance of Gly-GO/g-C$_3$N$_4$ membrane. (d) The effect of feed concentration on the separation performance of Gly-GO/g-C$_3$N$_4$ membrane, including total permeance, dye rejection, and dye permeation rate.

the permeance [48]. Fig. 8b depicts the separation performance of the Gly-GO/g-C$_3$N$_4$ membrane after HPEI coating treatment. Likewise, the membrane permeation continuously increased with increasing glycine content. Finally, the MB rejection of the Gly-GO/g-C$_3$N$_4$ composite membrane modified by 2 mL glycine was nearly 90% after being coated with HPEI (M.W. = 10,000), and the permeance was 25.8 L h^{-1} m^{-2} bar^{-1}. As illustrated in Fig. 8c, this phenomenon may occur because the modification of glycine led to a looser stacking of graphene sheets, thereby increasing the permeance due to low barrier while inevitably sacrificing MB rejection [18].

The pure water permeance of the GO, GO/g-C$_3$N$_4$, and Gly-GO/g-C$_3$N$_4$ membranes are compared in Fig. 9a. Similar to the above result in Fig. 6b, the introduction of g-C$_3$N$_4$ nanosheets reduced the size of the 2D nanochannels in the GO membrane, reducing the pure water permeance of the membrane from 46 L h^{-1} m^{-2} bar^{-1} to 23.7 L h^{-1} m^{-2} bar^{-1}. However, the pure water permeance of the Gly-GO/g-C$_3$N$_4$ membrane climbed to 206.8 L h^{-1} m^{-2} bar^{-1}. The high water permeance was close to the data obtained from the reported MOF/GO/CA (CA = cellulose acetate) composite membranes (183.5 L m^{-2} h^{-1}) [8], and was much larger than other small molecule modified GO membranes. For example, Zhang et al. reported inserting inorganic MoS$_2$ sheets into the interlayer of a GO membrane, but the penetration value was only 10.2 L h^{-1} m^{-2} bar^{-1} [49]. These values indicate that the introduction of glycine changed the layer spacing of laminates and greatly enhanced the water

transport capacity of the GO membrane, consistent with the illustrations shown in Figs. 6a and 8c. Furthermore, the effect of the pHs of the dye solutions on the separation performance of the Gly-GO/g-C$_3$N$_4$ membrane was investigated by adjusting the pHs of MB aqueous solutions from 4 to 10. As shown in Fig. 9c, the rejections of MB (molecular weight of 320 g/mol and size of 2 nm) remained between 80% to 90%, with a permeance of around 25 L h^{-1} m^{-2} bar^{-1} in most cases (pH of 5–10). However, at the low pH of 4, the rejection decreased to about 31%, probably due to acid etching of the Gly-GO/g-C$_3$N$_4$ structure. We also investigated the effect of feed concentration on separation performance. An increased dye concentration in the feed solution led to concentration polarization and increased osmotic pressure; therefore, the driving force of the solvent (*i.e.*, H$_2$O) decreased in a constant pressure operation [50]. Accordingly, as shown in Fig. 9d, the permeance decreased inevitably with an almost constant dye rejection. However, the permeation rate of MB (in the unit of mmol m^{-2} h^{-1}) showed an approximately linear relationship with its concentration in the feed due to the increased osmotic pressure.

3.2.4. Other dye retention performance

We also selected a series of dye molecules of different sizes and charges (see Fig. S10) for the evaluation of the separation performance of our prepared Gly-GO/g-C$_3$N$_4$/HPEI composite membranes, which are summarized in Fig. 9b. We found that both the molecular size and
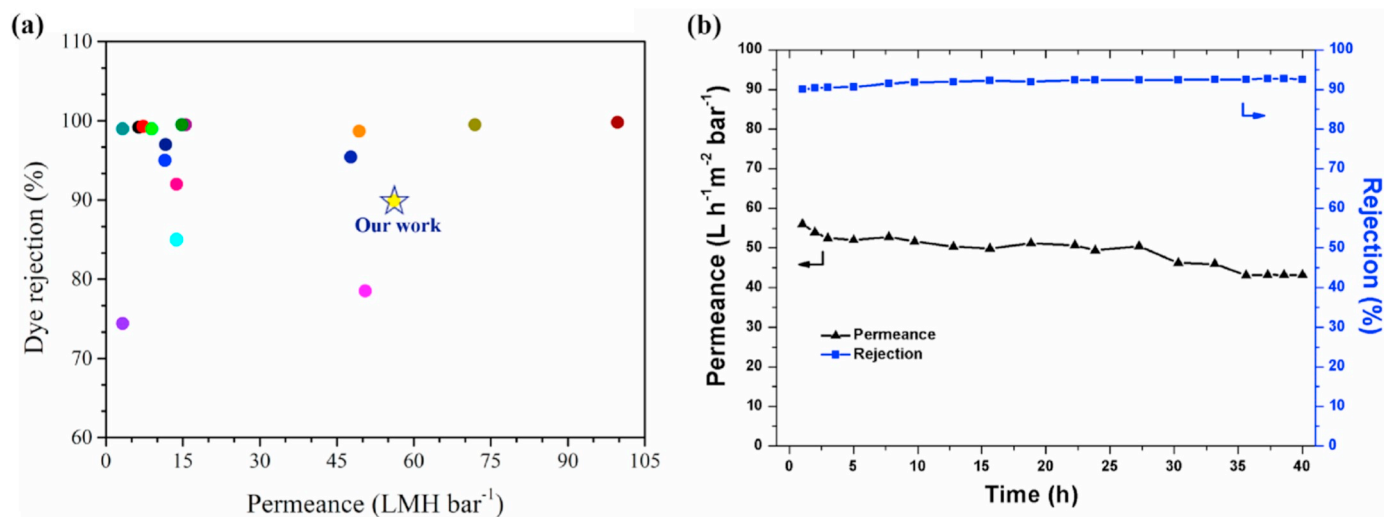
Fig. 10. (a) Comparison of the separation performance among our prepared membranes and other reported GO-based membranes in literature. Refer to the detailed data in Table S2. (b) The long-term separation performance of the Gly-GO/g-C$_3$N$_4$ membrane towards AB over the 40 h testing period.

electrostatic charge of dye molecules significantly affected their retention. Similar to MB, both RhB and AB are positively charged, and they share a repulsive force for the membrane surface. Therefore, the rejection of RhB (M.W. = 479.0) and AB (M.W. = 1298.9) reached 77.7% and 89.5%, respectively. By comparison, EY (M.W. = 647.9) and EB (M.W. = 960.8) are much larger than MB (M.W. = 319.9), and their rejection was 91.1% and 99.4% while maintaining a total permeance of 15.7 and 42.9 L h^{-1} m^{-2} bar^{-1}, respectively. Nevertheless, EY and EB are anionic dyes, thus their adsorption at the initial time point was one of the reasons for their high rejection (see Fig. S11). However, based on the adsorption equilibrium, a high rejection could be maintained and the dyes were concentrated in the feed side, indicating the molecular sieve effect of the designed membranes [49,51]. We also compared the separation performance of our prepared membranes with other reported GO membranes, as shown in Fig. 10a and Table S2. The obtained Gly-GO/g-C$_3$N$_4$ membrane had a higher water penetration (56.1 L h^{-1} m^{-2} bar^{-1}) than most GO membrane while maintaining high retention of organic dyes. These results suggest that glycine molecules play a synergistic role with GO/g-C$_3$N$_4$, contributing to the enhanced separation performance of GO-based membrane [18,52–62]. The long-term stability of the Gly-GO/g-C$_3$N$_4$ membrane was further investigated and the results are summarized in Fig. 10b. It was found that the membrane yielded 90%–93% dye rejection over a 40 h testing period, indicating acceptable stability. The permeance declined slightly and reached a steady value of 43.2 L h^{-1} m^{-2} bar^{-1}, probably due to concentration polarization or fouling on the membrane surface [63].

4. Conclusions

In this study, we successfully prepared a series of GO/g-C$_3$N$_4$ composite membranes by glycine modification for nanofiltration. Both glycine and g-C$_3$N$_4$ were intercalated between the GO nanosheets by covalent and non-covalent interactions, respectively. The resulting tightly assembled membranes had enlarged interlayer spacing and larger transport channels for water transportation while retaining good solute retention (*viz.*, organic dyes). Both XPS and FTIR results confirm the successful grafting of glycine on the GO membranes. After the further surface modification of the composite membrane by HPEI, the separation performance was further enhanced, suggesting both physical sieving and electrostatic interaction contributed to the high dye rejection observed. In summary, this study combines both non-covalent and covalent interactions to modify GO membranes, which not only improves the separation performance of GO membranes but also provides a

simple solution-based strategy for the fabrication of GO membranes for the water purification field.

Declaration of competing interest

The authors declare that they have no known competing financial interests or personal relationships that could have appeared to influence the work reported in this paper.

CRediT authorship contribution statement

Zhitao Wu: Conceptualization, Investigation, Writing - original draft. **Le Gao:** Investigation. **Jie Wang:** Data curation. **Feigang Zhao:** Methodology. **Longlong Fan:** Methodology. **Dan Hua:** Supervision, Conceptualization. **Susilo Japip:** Data curation. **Jingran Xiao:** Data curation. **Xueji Zhang:** Visualization. **Shu-Feng Zhou:** Resources, Conceptualization. **Guowu Zhan:** Writing - review & editing, Supervision, Conceptualization.

Appendix A. Supplementary data

Supplementary data to this article can be found online at https://doi.org/10.1016/j.memsci.2020.117948.

References

[1] Y. Wang, L. Liu, J. Hong, J. Cao, C. Deng, A novel Fe(OH)$_3$/g-C$_3$N$_4$ composite membrane for high efficiency water purification, J. Membr. Sci. 564 (2018) 372–381.

[2] C. Buelke, A. Alshami, J. Casler, Y. Lin, M. Hickner, I.H. Aljundi, Evaluating graphene oxide and holey graphene oxide membrane performance for water purification, J. Membr. Sci. 588 (2019) 117195.

[3] D.I. Petukhov, E.A. Chernova, O.O. Kapitanova, O.V. Boytsova, R.G. Valeev, A. P. Chumakov, O.V. Konovalov, A.A. Eliseev, Thin graphene oxide membranes for gas dehumidification, J. Membr. Sci. 577 (2019) 184–194.

[4] T. Bayer, R. Selyanchyn, S. Fujikawa, K. Sasaki, S.M. Lyth, Spray-painted graphene oxide membrane fuel cells, J. Membr. Sci. 541 (2017) 347–357.

[5] H. Lee, J. Han, K. Kim, J. Kim, E. Kim, H. Shin, J.-C. Lee, Highly sulfonated polymer-grafted graphene oxide composite membranes for proton exchange membrane fuel cells, J. Ind. Eng. Chem. 74 (2019) 223–232.

[6] M.D. Stoller, S. Park, Y. Zhu, J. An, R.S. Ruoff, Graphene-based ultracapacitors, Nano Lett. 8 (2008) 3498–3502.

[7] Y. Gao, K. Su, Z. Li, B. Cheng, Graphene oxide hybrid poly(p-phenylene sulfide) nanofiltration membrane intercalated by bis(triethoxysilyl) ethane, Chem. Eng. J. 352 (2018) 10–19.

[8] S. Yang, Q. Zou, T. Wang, L. Zhang, Effects of GO and MOF@GO on the permeation and antifouling properties of cellulose acetate ultrafiltration membrane, J. Membr. Sci. 569 (2019) 48–59.

[9] L. Huang, Y. Li, Q. Zhou, W. Yuan, G. Shi, Graphene oxide membranes with tunable semipermeability in organic solvents, Adv. Mater. 27 (2015) 3797–3802.

[10] D. Hua, T.-S. Chung, Polyelectrolyte functionalized lamellar graphene oxide membranes on polypropylene support for organic solvent nanofiltration, Carbon 122 (2017) 604–613.

[11] Y. Yang, X. Yang, L. Liang, Y. Gao, H. Cheng, X. Li, M. Zou, R. Ma, Q. Yuan, X. Duan, Large-area graphene-nanomesh/carbon-nanotube hybrid membranes for ionic and molecular nanofiltration, Science 364 (2019) 1057.

[12] R.R. Nair, H.A. Wu, P.N. Jayaram, I.V. Grigorieva, A.K. Geim, Unimpeded permeation of water through helium-leak–tight graphene-based membranes, Science 335 (2012) 442.

[13] H. Zhao, J. Yang, Z. Li, Y. Geng, S. He, M. Chen, R. Li, Q. Li, L. Zhang, Effect of cations on stabilizing graphene oxide membranes in aqueous solutions, Appl. Surf. Sci. 487 (2019) 962–971.

[14] Y. Han, Z. Xu, C. Gao, Ultrathin graphene nanofiltration membrane for water purification, Adv. Funct. Mater. 23 (2013) 3693–3700.

[15] K. Goh, L. Setiawan, L. Wei, R. Si, A.G. Fane, R. Wang, Y. Chen, Graphene oxide as effective selective barriers on a hollow fiber membrane for water treatment process, J. Membr. Sci. 474 (2015) 244–253.

[16] M. Sun, J. Li, Graphene oxide membranes: functional structures, preparation and environmental applications, Nano Today 20 (2018) 121–137.

[17] Y. Li, H. Zhang, P. Liu, D. Wang, Y. Li, H. Zhao, Cross-linked g-C₃N₄/rGO nanocomposites with tunable band structure and enhanced visible light photocatalytic activity, Small 9 (2013) 3336–3344.

[18] L. Chen, N. Li, Z. Wen, L. Zhang, Q. Chen, L. Chen, P. Si, J. Feng, Y. Li, J. Lou, L. Ci, Graphene oxide based membrane intercalated by nanoparticles for high performance nanofiltration application, Chem. Eng. J. 347 (2018) 12–18.

[19] J. Ran, C. Chu, T. Pan, L. Ding, P. Cui, C.-F. Fu, C.-L. Zhang, T. Xu, Non-covalent cross-linking to boost the stability and permeability of graphene-oxide-based membranes, J. Mater. Chem. 7 (2019) 8085–8091.

[20] W.-S. Hung, C.-H. Tsou, M. De Guzman, Q.-F. An, Y.-L. Liu, Y.-M. Zhang, C.-C. Hu, K.-R. Lee, J.-Y. Lai, Cross-Linking with diamine monomers to prepare composite graphene oxide-framework membranes with varying d-spacing, Chem. Mater. 26 (2014) 2983–2990.

[21] L. Qu, G. Zhu, J. Ji, T.P. Yadav, Y. Chen, G. Yang, H. Xu, H. Li, Recyclable visible light-driven O-g-C₃N₄/graphene oxide/N-carbon nanotube membrane for efficient removal of organic pollutants, ACS Appl. Mater. Interfaces 10 (2018) 42427–42435.

[22] Y. Wei, Y. Zhu, Y. Jiang, Photocatalytic self-cleaning carbon nitride nanotube intercalated reduced graphene oxide membranes for enhanced water purification, Chem. Eng. J. 356 (2019) 915–925.

[23] F. Li, Z. Yu, H. Shi, Q. Yang, Q. Chen, Y. Pan, G. Zeng, L. Yan, A Mussel-inspired method to fabricate reduced graphene oxide/g-C₃N₄ composites membranes for catalytic decomposition and oil-in-water emulsion separation, Chem. Eng. J. 322 (2017) 33–45.

[24] Y. Wang, L. Li, Y. Wei, J. Xue, H. Chen, L. Ding, J. Caro, H. Wang, Water transport with ultralow friction through partially exfoliated g-C₃N₄ nanosheet membranes with self-supporting spacers, Angew. Chem. Int. Ed. 56 (2017) 8974–8980.

[25] M.-m. Cheng, L.-j. Huang, Y.-x. Wang, Y.-c. Zhao, J.-g. Tang, Y. Wang, Y. Zhang, M. Hedayati, M.J. Kipper, S.R. Wickramasinghe, Synthesis of graphene oxide/polyacrylamide composite membranes for organic dyes/water separation in water purification, J. Mater. Sci. 54 (2019) 252–264.

[26] J. Jiang, L. Ou-yang, L. Zhu, A. Zheng, J. Zou, X. Yi, H. Tang, Dependence of electronic structure of g-C₃N₄ on the layer number of its nanosheets: a study by Raman spectroscopy coupled with first-principles calculations, Carbon 80 (2014) 213–221.

[27] C. Cao, M. Daly, C.V. Singh, Y. Sun, T. Filleter, High strength measurement of monolayer graphene oxide, Carbon 81 (2015) 497–504.

[28] D. Zhao, J. Zhao, Y. Ji, G. Liu, S. Liu, W. Jin, Facilitated water-selective permeation via PEGylation of graphene oxide membrane, J. Membr. Sci. 567 (2018) 311–320.

[29] L. Huang, J. Chen, T. Gao, M. Zhang, Y. Li, L. Dai, L. Qu, G. Shi, Reduced graphene oxide membranes for ultrafast organic solvent nanofiltration, Adv. Mater. 28 (2016) 8669–8674.

[30] Y. Zhan, S. He, X. Wan, S. Zhao, Y. Bai, Thermally and chemically stable poly (arylene ether nitrile)/halloysite nanotubes intercalated graphene oxide nanofibrous composite membranes for highly efficient oil/water emulsion separation in harsh environment, J. Membr. Sci. 567 (2018) 76–88.

[31] J. Zhao, Y. Zhu, G. He, R. Xing, F. Pan, Z. Jiang, P. Zhang, X. Cao, B. Wang, Incorporating zwitterionic graphene oxides into sodium alginate membrane for

[32] efficient water/alcohol separation, ACS Appl. Mater. Interfaces 8 (2016) 2097–2103.

[32] Y. Wu, F. Wang, X. Li, J. He, Y. Huang, Fabrication of a graphene oxide/nanoscale aramid fiber composite membrane with improved hydrophilicity and mechanical strength via a fast-drying method using absolute ethanol as proton donor, J. Mater. Sci. 53 (2018) 16383–16392.

[33] A. Karkooti, A.Z. Yazdi, P. Chen, M. McGregor, N. Nazemifard, M. Sadrzadeh, Development of advanced nanocomposite membranes using graphene nanoribbons and nanosheets for water treatment, J. Membr. Sci. 560 (2018) 97–107.

[34] S. Deng, V. Tjoa, H.M. Fan, H.R. Tan, D.C. Sayle, M. Olivo, S. Mhaisalkar, J. Wei, C. H. Sow, Reduced graphene oxide conjugated Cu₂O nanowire mesocrystals for high-performance NO₂ gas sensor, J. Am. Chem. Soc. 134 (2012) 4905–4917.

[35] L. Zhang, B. Chen, A. Ghaffar, X. Zhu, Nanocomposite membrane with polyethylenimine-grafted graphene oxide as a novel additive to enhance pollutant filtration performance, Environ. Sci. Technol. 52 (2018) 5920–5930.

[36] Z. Zhang, Z. Kang, H. Yu, Y. Jin, Y. Cao, From reverse osmosis to nanofiltration: precise control of the pore size and charge of polyamide membranes via interfacial polymerization, Desalination 466 (2019) 16–23.

[37] F. Zhao, L. Fan, K. Xu, D. Hua, G. Zhan, S.-F. Zhou, Hierarchical sheet-like Cu/Zn/ Al nanocatalysts derived from LDH/MOF composites for CO₂ hydrogenation to methanol, J. CO₂ Util. 33 (2019) 222–232.

[38] N. Meng, R.C.E. Priestley, Y. Zhang, H. Wang, X. Zhang, The effect of reduction degree of GO nanosheets on microstructure and performance of PVDF/GO hybrid membranes, J. Membr. Sci. 501 (2016) 169–178.

[39] X. Yang, F. Qian, G. Zou, M. Li, J. Lu, Y. Li, M. Bao, Facile fabrication of acidified g-C₃N₄/g-C₃N₄ hybrids with enhanced photocatalysis performance under visible light irradiation, Appl. Catal., B 193 (2016) 22–35.

[40] P. Zhang, J.-L. Gong, G.-M. Zeng, C.-H. Deng, H.-C. Yang, H.-Y. Liu, S.-Y. Huan, Cross-linking to prepare composite graphene oxide-framework membranes with high-flux for dyes and heavy metal ions removal, Chem. Eng. J. 322 (2017) 657–666.

[41] L. Ge, C. Han, Synthesis of MWNTs/g-C₃N₄ composite photocatalysts with efficient visible light photocatalytic hydrogen evolution activity, Appl. Catal., B 117–118 (2012) 268–274.

[42] L. Qu, W. Wang, H. Xu, W. Wang, Y. Liu, L. Kuo, T.P. Yadav, J. Wu, J. Joyner, Y. Song, H. Li, J. Lou, R. Vajtai, P.M. Ajayan, Gold nanoparticles and g-C₃N₄-intercalated graphene oxide membrane for recyclable surface enhanced Raman scattering, Adv. Funct. Mater. 27 (2017) 1701714.

[43] W.-J. Ong, L.-L. Tan, S.-P. Chai, S.-T. Yong, A.R. Mohamed, Surface charge modification via protonation of graphitic carbon nitride (g-C₃N₄) for electrostatic self-assembly construction of 2D/2D reduced graphene oxide (rGO)/g-C₃N₄ nanostructures toward enhanced photocatalytic reduction of carbon dioxide to methane, Nano Energy 13 (2015) 757–770.

[44] Y.C. Xu, Z.X. Wang, X.Q. Cheng, Y.C. Xiao, L. Shao, Positively charged nanofiltration membranes via economically mussel-substance-simulated co-deposition for textile wastewater treatment, Chem. Eng. J. 303 (2016) 555–564.

[45] X. Wang, H. Wang, Y. Wang, J. Gao, J. Liu, Y. Zhang, Hydrotalcite/graphene oxide hybrid nanosheets functionalized nanofiltration membrane for desalination, Desalination 451 (2019) 209–218.

[46] H. Chen, W.S. Hung, C.H. Lo, S.H. Huang, M.L. Cheng, G. Liu, K.R. Lee, J.Y. Lai, Y. M. Sun, C.C. Hu, R. Suzuki, T. Ohdaira, N. Oshima, Y.C. Jean, Free-volume depth profile of polymeric membranes studied by positron annihilation spectroscopy: layer structure from interfacial polymerization, Macromolecules 40 (2007) 7542–7557.

[47] Y.P. Tang, D.R. Paul, T.S. Chung, Free-standing graphene oxide thin films assembled by a pressurized ultrafiltration method for dehydration of ethanol, J. Membr. Sci. 458 (2014) 199–208.

[48] R.S.A. De Lange, K. Keizer, A.J. Burggraaf, Characterization of microporous non-supported membrane top-layers using physisorption techniques, J. Porous Mater. 1 (1995) 139–153.

[49] P. Zhang, J.-L. Gong, G.-M. Zeng, B. Song, W. Cao, H.-Y. Liu, S.-Y. Huan, P. Peng, Novel "loose" GO/MoS₂ composites membranes with enhanced permeability for effective salts and dyes rejection at low pressure, J. Membr. Sci. 574 (2019) 112–123.

[50] Y. He, G. Li, H. Wang, J. Zhao, H. Su, Q. Huang, Effect of operating conditions on separation performance of reactive dye solution with membrane process, J. Membr. Sci. 321 (2008) 183–189.

[51] D. Hua, S. Japip, K.Y. Wang, T.-S. Chung, Green design of poly(m-phenylene isophthalamide)-based thin-film composite membranes for organic solvent nanofiltration and concentrating lecithin in hexane, ACS Sustain. Chem. Eng. 6 (2018) 10696–10705.

[52] G. Abdi, A. Alizadeh, S. Zinadini, G. Moradi, Removal of dye and heavy metal ion using a novel synthetic polyethersulfone nanofiltration membrane modified by magnetic graphene oxide/metformin hybrid, J. Membr. Sci. 552 (2018) 326–335.

[53] L. Chen, Y. Li, L. Chen, N. Li, C. Dong, Q. Chen, B. Liu, Q. Ai, P. Si, J. Feng, L. Zhang, J. Suhr, J. Lou, L. Ci, A large-area free-standing graphene oxide multilayer membrane with high stability for nanofiltration applications, Chem. Eng. J. 345 (2018) 536–544.

[54] D. Ji, C. Xiao, S. An, J. Zhao, J. Hao, K. Chen, Preparation of high-flux PSF/GO loose nanofiltration hollow fiber membranes with dense-loose structure for treating textile wastewater, Chem. Eng. J. 363 (2019) 33–42.

[55] H. Kang, J. Shi, L. Liu, M. Shan, Z. Xu, N. Li, J. Li, H. Lv, X. Qian, L. Zhao, Sandwich morphology and superior dye-removal performances for nanofiltration membranes self-assemblied via graphene oxide and carbon nanotubes, Appl. Surf. Sci. 428 (2018) 990–999.

[56] T. Liu, X. Liu, N. Graham, W. Yu, K. Sun, Two-dimensional MXene incorporated graphene oxide composite membrane with enhanced water purification performance, J. Membr. Sci. 593 (2020) 117431.

[57] J. Sun, C. Hu, Z. Liu, H. Liu, J. Qu, Surface charge and hydrophilicity improvement of graphene membranes via modification of pore surface oxygen-containing groups to enhance permeability and selectivity, Carbon 145 (2019) 140–148.

[58] C.-Y. Wang, W.-J. Zeng, T.-T. Jiang, X. Chen, X.-L. Zhang, Incorporating attapulgite nanorods into graphene oxide nanofiltration membranes for efficient dyes wastewater treatment, Separ. Purif. Technol. 214 (2019) 21–30.

[59] L. Wang, N. Wang, J. Li, J. Li, W. Bian, S. Ji, Layer-by-layer self-assembly of polycation/GO nanofiltration membrane with enhanced stability and fouling resistance, Separ. Purif. Technol. 160 (2016) 123–131.

[60] Y. Zhan, X. Wan, S. He, Q. Yang, Y. He, Design of durable and efficient poly(arylene ether nitrile)/bioinspired polydopamine coated graphene oxide nanofibrous composite membrane for anionic dyes separation, Chem. Eng. J. 333 (2018) 132–145.

[61] M. Zhang, J. Sun, Y. Mao, G. Liu, W. Jin, Effect of substrate on formation and nanofiltration performance of graphene oxide membranes, J. Membr. Sci. 574 (2019) 196–204.

[62] Y. Zhang, S. Japip, T.-S. Chung, Thermally evolved and boron bridged graphene oxide (GO) frameworks constructed on microporous hollow fiber substrates for water and organic matters separation, Carbon 123 (2017) 193–204.

[63] S.-P. Sun, T.-S. Chung, K.-J. Lu, S.-Y. Chan, Enhancement of flux and solvent stability of Matrimid® thin-film composite membranes for organic solvent nanofiltration, AIChE J. 60 (2014) 3623–3633.